SC-Corr Code Package:
Theory and Reference Manual

Matthew S. Church
Ananth Group
Cornell University
msc336@cornell.edu
Version 1.1

December 12, 2017

This document serves as a reference manual for the SC-Corr Code Package (FORTRAN) developed by M. S. Church, S. V. Antipov and N. Ananth on the Ananth group GitHub page. Also see the Ananth Group website. The package contains a variety of methods that compute the real-time correlation function within the framework of the semiclassical initial value representation. This document provides some theoretical background and useful references for additional reading, outlines the structure of the program, and describes how it can be used or altered.

Contents

1 Introduction

Semiclassical initial value representation (SC-IVR) based methods are a promising approach to simulating complex chemical systems in real-time; they are rigorously derived, describe quantum effects accurately, and employ near-classical trajectories. The aim of this program is to provide several means of computing the real-time correlation function using methods that are based on the SC-IVR formalism. We provide simple 1D and 2D model systems with which to test and become familiar with the program, although the code is general and extensions to arbitrary multidimensional systems can be easily implemented, as described below. Section II of this manual provides some brief theoretical background for the different SC-IVR methods used, and Section III provides a description of the program structure as well as some useful tutorials.

1.1 Useful References

Textbooks:
1. D. Tannor "Introduction to Quantum Mechanics: A Time Dependent Perspective" Univ. Sci. Books, Chapter 10 (2007)
2. M.S. Child "Semiclassical Mechanics with Molecular Applications" Oxford University Press 2^{nd} Ed.(2014)
3. M.C. Gutzwiller "Chaos in Classical and Quantum Mechanics" Springer-Verlag (1990)
Journal Articles
4. W.H. Miller, J. Phys. Chem. A. **105**, 2942 (2001)
5. M. Thoss and H. Wang, Annu. Rev. Phys. Chem. **55**, 299 (2004)
6. S.V. Antipov, Z. Ye, and N. Ananth, J. Chem. Phys. **142**, 184102 (2015)
7. M.S. Church, S.V. Antipov, and N. Ananth, J. Chem. Phys. **146**, 234104 (2017)
8. M.S. Church, T.J.H. Hele, G.S. Ezra, and N. Ananth. J. Chem. Phys. **148**, 102326 (2018)

*Note: We particularly recommend Ref. 1 as an introduction to semiclassical ideas.

2 Semiclassical Propagators

2.1 Van Vleck-Gutzwiller Propagator

We begin with a brief discussion of semiclassical propagators. Using the Feynman path integral formulation of quantum mechanics, the amplitude associated with a transition from position state $|\mathbf{q}_0\rangle$ to $|\mathbf{q}_t\rangle$ in time t is given by

$$\langle \mathbf{q}_t | e^{-\frac{i}{\hbar}\hat{H}t} | \mathbf{q}_0 \rangle \;=\; \int D[\mathbf{q}(t)]\; e^{\frac{i}{\hbar}S[\mathbf{q}(t)]} \tag{1}$$

where $S[\mathbf{q}(t)]$ is the action integral associated with path $\mathbf{q}(t)$, $D[\mathbf{q}(t)]$ is the path differential, and $\hat{H}$ is the Hamiltonian. The oscillatory phase on the right hand side of Eq. (1) suggests that stationary paths (i.e. the classical paths, according to Hamilton's principle) contribute the most to the transition amplitude whereas non-classical paths exhibit significant phase cancellation leading to lower contributions. Expanding $S[\mathbf{q}(t)]$ around the classical paths to second order and evaluating the integral analytically leads to the Van Vleck-Gutzwiller propagator (VVG),

$$\langle \mathbf{q}_t | e^{-\frac{i}{\hbar}\hat{H}t} | \mathbf{q}_0 \rangle_{SC} \;=\; \sum_{\text{classical paths}} \sqrt{\frac{1}{(2\pi i\hbar)^N} \det \left| \frac{\partial \mathbf{q}_t}{\partial \mathbf{p}_0} \right|^{-1}}\; e^{\frac{i}{\hbar}S[\mathbf{q}(t)]}, \tag{2}$$

where $\mathbf{p}_0$ is the initial momentum. Since Eq. (2) is obtained as the stationary phase approximation to the exact propagator, it is a valid replacement for Eq. (1) in the limit $\hbar \to 0$. Although SC methods have been shown to capture most important quantum effects, there are practical challenges to consider when computing Eq. (2). Finding all trajectories that satisfy the double-ended boundary condition requires an exhaustive and computationally inefficient search, and the prefactor may diverge when the determinant of the $N \times N$ matrix $\frac{\partial \mathbf{q}_t}{\partial \mathbf{p}_0}$ approaches zero, among others.

2.2 Position-space (Van Vleck) SC-IVR

The trajectory search problem that arises from computing Eq. (2) can be removed by formulating the propagator in terms of an integral over initial phase space conditions. Using completeness to express the time evolution operator,

$$e^{-\frac{i}{\hbar}\hat{H}t} \;=\; \int \mathrm{d}\mathbf{q}_t \int \mathrm{d}\mathbf{q}_0 \, |\mathbf{q}_t\rangle \langle \mathbf{q}_t | e^{-\frac{i}{\hbar}\hat{H}t} | \mathbf{q}_0 \rangle \langle \mathbf{q}_0 | \,,$$

and then substituting the expression in Eq. (2) for the transition amplitude we obtain,

$$e^{-\frac{i}{\hbar}\hat{H}t} \approx \frac{1}{(2\pi i\hbar)^{\frac{N}{2}}} \sum_{\text{classical paths}} \int \mathrm{d}\mathbf{q}_t \int \mathrm{d}\mathbf{q}_0 \, \det \left| \frac{\partial \mathbf{q}_t}{\partial \mathbf{p}_0} \right|^{-\frac{1}{2}} e^{\frac{i}{\hbar} S_t(\mathbf{p}_0, \mathbf{q}_0)} \, |\mathbf{q}_t\rangle \langle \mathbf{q}_0| \,. \tag{3}$$

Now, a simple change of variables to replace the integral over position at time t in Eq. 3 with initial momentum,

$$\sum_{\text{classical paths}} \int \mathrm{d}\mathbf{q}_t \;=\; \int \mathrm{d}\mathbf{p}_0 \left| \frac{\partial \mathbf{q}_t}{\partial \mathbf{p}_0} \right|,$$

leads to the Van Vleck-IVR (VV-IVR) expression for the propagator,

$$e^{-\frac{i}{\hbar}\hat{H}t} \;\approx\; \frac{1}{(2\pi i\hbar)^{\frac{N}{2}}} \int \mathrm{d}\mathbf{p}_0 \int \mathrm{d}\mathbf{q}_0 \, \det \left| \frac{\partial \mathbf{q}_t}{\partial \mathbf{p}_0} \right|^{\frac{1}{2}} e^{\frac{i}{\hbar} S_t(\mathbf{p}_0, \mathbf{q}_0)} \, |\mathbf{q}_t\rangle \langle \mathbf{q}_0| \,. \tag{4}$$

Though the conversion removes the double-ended boundary condition and moves the prefactor to the numerator, evaluating Eq. (4) remains challenging for multidimensional systems due to the oscillatory phase and lack of initial momentum information.

We note that VV-IVR propagator can also be written in terms of momentum states as

$$e^{-\frac{i}{\hbar}\hat{H}t} \;\approx\; \frac{1}{(2\pi i\hbar)^{\frac{N}{2}}} \int \mathrm{d}\mathbf{p}_0 \int \mathrm{d}\mathbf{q}_0 \, \det \left| \frac{\partial \mathbf{p}_t}{\partial \mathbf{q}_0} \right|^{\frac{1}{2}} e^{\frac{i}{\hbar} S_t(\mathbf{p}_0, \mathbf{q}_0)} \, |\mathbf{p}_t\rangle \langle \mathbf{p}_0| \,. \tag{5}$$

2.3 Coherent State (Herman-Kluk) SC-IVR

An additional complexity in evaluating the integrals in Eq. (4)/Eq. (5) arises from the lack of an obvious Monte Carlo sampling function for momentum/position respectively. An appealing alternative is the Herman Kluk-IVR (HK-IVR), where the semiclassical propagator is constructed in a basis of coherent states

$$e^{-\frac{i}{\hbar}\hat{H}t} \;\approx\; \frac{1}{(2\pi\hbar)^{N}} \int \mathrm{d}\mathbf{p}_0 \int \mathrm{d}\mathbf{q}_0 \, C_t(\mathbf{p}_0, \mathbf{q}_0) \, e^{\frac{i}{\hbar} S_t(\mathbf{p}_0, \mathbf{q}_0)} \, |\mathbf{p}_t \mathbf{q}_t\rangle \langle \mathbf{p}_0 \mathbf{q}_0| \,. \tag{6}$$

The prefactor here is given by

$$C_t(\mathbf{p}_0,\mathbf{q}_0) \;=\; \det\left|\gamma_t^{\frac{1}{2}}\mathbf{M}_{qq}\gamma_0^{-\frac{1}{2}} + \gamma_t^{-\frac{1}{2}}\mathbf{M}_{pp}\gamma_0^{\frac{1}{2}} - i\hbar\gamma_t^{\frac{1}{2}}\mathbf{M}_{qp}\gamma_0^{\frac{1}{2}} + \frac{i}{\hbar}\gamma_t^{-\frac{1}{2}}\mathbf{M}_{pq}\gamma_0^{-\frac{1}{2}}\right|^{\frac{1}{2}},$$

and $\mathbf{M}_{\alpha\beta} = \frac{\partial\alpha_t}{\partial\beta_0}$, and γ_t is an $N\times N$ diagonal matrix describing the width of the coherent states. The coherent state wavefunctions in Eq. (6) are given by,

$$\psi(\bar{\mathbf{x}}) \;=\; \langle\bar{\mathbf{x}}|\mathbf{q}\,\mathbf{p}\rangle = \left(\frac{\det|\gamma|}{\pi^N}\right)^{\frac{1}{4}} e^{-\frac{1}{2}(\bar{\mathbf{x}}-\mathbf{q})\cdot\gamma\cdot(\bar{\mathbf{x}}-\mathbf{q})+\frac{i}{\hbar}\mathbf{p}\cdot(\bar{\mathbf{x}}-\mathbf{q})} \tag{7}$$

$$\tilde{\psi}(\bar{\mathbf{p}}) \;=\; \langle\bar{\mathbf{p}}|\mathbf{q}\,\mathbf{p}\rangle = \left(\frac{1}{\det|\gamma|\pi^N}\right)^{\frac{1}{4}} e^{-\frac{1}{2}(\bar{\mathbf{p}}-\mathbf{p})\cdot\gamma^{-1}\cdot(\bar{\mathbf{p}}-\mathbf{p})-\frac{i}{\hbar}\bar{\mathbf{p}}\cdot\mathbf{q}}, \tag{8}$$

HK-IVR is favorable over Eq. (4) or Eq. (5) from a practical standpoint since the integrals to be evaluated involve Gaussian forms, and because the coherent state overlap terms provide a convenient choice for importance sampling both initial positions and momenta $(\mathbf{p}_0,\mathbf{q}_0)$,

$$\begin{aligned}\langle\mathbf{p}_0'\,\mathbf{q}_0'|\mathbf{p}_0\,\mathbf{q}_0\rangle \;&= e^{-\frac{1}{4}(\mathbf{q}_0'-\mathbf{q}_0)\cdot\gamma\cdot(\mathbf{q}_0'-\mathbf{q}_0)}\\ &\times e^{-\frac{1}{4\hbar^2}(\mathbf{p}_0'-\mathbf{p}_0)\cdot\gamma^{-1}\cdot(\mathbf{p}_0'-\mathbf{p}_0)}\\ &\times e^{\frac{i}{2\hbar}(\mathbf{p}_0'+\mathbf{p}_0)\cdot(\mathbf{q}_0'-\mathbf{q}_0)}.\end{aligned} \tag{9}$$

3 SC-IVR Correlation Functions

We are interested in computing real-time correlation functions of the form

$$C_{AB}(t) \;=\; \mathrm{Tr}\left[\hat{A}\,e^{\frac{i}{\hbar}\hat{H}t}\hat{B}\,e^{-\frac{i}{\hbar}\hat{H}t}\right], \tag{10}$$

with operator $\hat{A}$ typically representing the initial state of the system, and operator $\hat{B}$ representing the observable. The SC-IVR correlation function is obtained by substituting the quantum propagators with the corresponding SC approximations outlined above. The double Van Vleck representation (DVV-IVR) is then,

$$\begin{aligned}C_{AB}(t) \;&= \frac{1}{(2\pi\hbar)^N}\int\mathrm{d}\mathbf{p}_0\int\mathrm{d}\mathbf{q}_0\int\mathrm{d}\mathbf{p}_t'\int\mathrm{d}\mathbf{q}_t'\,e^{\frac{i}{\hbar}[S_t(\mathbf{p}_0,\mathbf{q}_0)+S_{-t}(\mathbf{p}_t,\mathbf{q}_t)]}\\ &\times\det\left|\mathbf{M}_{qp}\,\mathbf{M}_{qp}^{'}\right|^{\frac{1}{2}}\langle\mathbf{q}_0|\hat{A}|\mathbf{q}_0'\rangle\,\langle\mathbf{q}_t'|\hat{B}|\mathbf{q}_t\rangle\end{aligned} \tag{11}$$

with $(\mathbf{p}_0,\mathbf{q}_0)$ and $(\mathbf{p}_t',\mathbf{q}_t')$ the initial conditions of a forward and backward trajectory, respectively. Similarly, the momentum representation is given by

$$\begin{aligned}C_{AB}(t) \;&= \frac{1}{(2\pi i\hbar)^N}\int\mathrm{d}\mathbf{p}_0\int\mathrm{d}\mathbf{q}_0\int\mathrm{d}\mathbf{p}_t'\int\mathrm{d}\mathbf{q}_t'\,e^{\frac{i}{\hbar}[S_t(\mathbf{p}_0,\mathbf{q}_0)+S_{-t}(\mathbf{p}_t,\mathbf{q}_t)]}\\ &\times\det\left|\mathbf{M}_{pq}\,\mathbf{M}_{pq}^{'}\right|^{\frac{1}{2}}\langle\mathbf{p}_0|\hat{A}|\mathbf{p}_0'\rangle\,\langle\mathbf{p}_t'|\hat{B}|\mathbf{p}_t\rangle\,.\end{aligned} \tag{12}$$

Finally there is the Double Herman-Kluk correlation function (DHK-IVR),

$$\begin{aligned}C_{AB}(t) \;&= \frac{1}{(2\pi i\hbar)^{2N}}\int\mathrm{d}\mathbf{p}_0\int\mathrm{d}\mathbf{q}_0\int\mathrm{d}\mathbf{p}_t'\int\mathrm{d}\mathbf{q}_t'\,e^{\frac{i}{\hbar}[S_t(\mathbf{p}_0,\mathbf{q}_0)+S_{-t}(\mathbf{p}_t,\mathbf{q}_t)]}\\ &\times C_t(\mathbf{p}_0,\mathbf{q}_0)C_{-t}(\mathbf{p}_t',\mathbf{q}_t')\,\langle\mathbf{p}_0\mathbf{q}_0|\hat{A}|\mathbf{p}_0'\mathbf{q}_0'\rangle\,\langle\mathbf{p}_t'\mathbf{q}_t'|\hat{B}|\mathbf{p}_t\mathbf{q}_t\rangle\,.\end{aligned} \tag{13}$$

Though each of these representations can, formally, capture all important quantum effects, the oscillatory phase factors makes convergence difficult and often impossible to achieve for large dimensional systems. It is clear that additional approximations are required to extend the applicability of these methods to complex systems.

3.1 Linearized SC-IVR

The linearized approximation (LSC-IVR) assumes that the forward and backward trajectories employed in calculating correlation functions as described in the section above are very close to each other. It is derived by taking Eq. (11) and converting to mean and difference variables: $\Delta_\alpha = \alpha_t^{'} + \alpha_t$, $\bar{\alpha} = \frac{1}{2}(\alpha_t^{'} + \alpha_t)$, with $\alpha = \mathbf{p}, \mathbf{q}$. Expanding all time-dependent quantities to first order in the difference variables, the expression reduces to a single phase space average over the Wigner distributions of the two operators evaluated at time zero and time t respectively,

$$C_{AB}(t) \;=\; \frac{1}{(2\pi\hbar)^N} \int \mathrm{d}\mathbf{p}_0 \int \mathrm{d}\mathbf{q}_0 \, A_w(\mathbf{p}_0, \mathbf{q}_0) \, B_w(\mathbf{p}_t, \mathbf{q}_t). \tag{14}$$

The Wigner distributions are given by

$$O_w(\mathbf{p}, \mathbf{q}) \;=\; \int \mathrm{d}\bar{\mathbf{q}} \, e^{-\frac{i}{\hbar}\mathbf{p}\cdot\bar{\mathbf{q}}} \left\langle \mathbf{q} + \frac{1}{2}\bar{\mathbf{q}} | \hat{O} | \mathbf{q} - \frac{1}{2}\bar{\mathbf{q}} \right\rangle . \tag{15}$$

LSC-IVR has found wide application in simulations of condensed phase systems, however, this method fails to capture quantum coherence effects.

3.2 Mixed Quantum-Classical IVR

DHK-IVR is then the most appealing approach to incorporate all quantum effects in MD simulations, but convergence is often difficult to achieve due to the oscillatory phase. The forward-backward trajectories interfere and give rise to a rapidly varying integrand, particularly where they are widely separated in phase space. This suggests that the overall contribution to the correlation function from such trajectory pairs is likely small due to phase cancellation.

An unfortunate consequence of this is that a large number of widely separated trajectory pairs must be considered to achieve convergence. We solve this problem by filtering the DHK-IVR such that trajectories with highly oscillatory phase contributions are effectively damped. The resulting Mixed Quantum-Classical (MQC)-IVR method significantly reduces the number of trajectories necessary to converge. The MQC-IVR expression is parametrically dependent on the strength of the filtration for a given system degree of freedom; a weak filter can accelerate convergence and reproduce accurate quantum effects, and a strong filter is equivalent to treating the system with a classical-limit theory that resembles LSC-IVR and is easily converged. The mode-specific parameterization allows for the treatment of different the modes of a system at different levels of SC theory between the classical and quantum limits.

Mathematically, we make the above approximation in the form of a modified Filinov transformation (MFT), which amounts to multiplying the integrand of Eq. (13) by a damping factor

$$F(\mathbf{z}\,;\mathbf{c}) \;=\; \det \left| \mathbb{I} + i\mathbf{c}\frac{\partial^2 \phi}{\partial \mathbf{z}^2} \right|^{\frac{1}{2}} e^{-\frac{1}{2}\frac{\partial \phi}{\partial \mathbf{z}}^T \mathbf{c} \frac{\partial \phi}{\partial \mathbf{z}}}, \tag{16}$$

which down-weights the regions of $\mathbf{z}$ (the variables of integration) where the integrand phase, $\phi(\mathbf{z})$, varies quickly. To derive the MQC-IVR, the damping factor is constructed specifically to damp the oscillations due to diverging trajectory pairs in the DHK-IVR expression for the real-time correlation function. The final result is given by

$$\begin{aligned} C_{AB}(t) \;=\; & \frac{1}{(2\pi\hbar)^{2N}} \int \mathrm{d}\mathbf{p}_0 \int \mathrm{d}\mathbf{q}_0 \int \mathrm{d}\boldsymbol{\Delta}_p \int \mathrm{d}\boldsymbol{\Delta}_q \, e^{\frac{i}{\hbar}[S_t(\mathbf{p}_0,\mathbf{q}_0) + S_{-t}(\mathbf{p}_t,\mathbf{q}_t)]} \\ & \times D_t(\mathbf{p}_0, \mathbf{q}_0, \boldsymbol{\Delta}_p, \boldsymbol{\Delta}_q; \mathbf{c}_p, \mathbf{c}_q) \left\langle \mathbf{p}_0 \mathbf{q}_0 | \hat{A} | \mathbf{p}_0^{'} \mathbf{q}_0^{'} \right\rangle \left\langle \mathbf{p}_t^{'} \mathbf{q}_t^{'} | \hat{B} | \mathbf{p}_t \mathbf{q}_t \right\rangle \\ & \times e^{-\frac{1}{2}\boldsymbol{\Delta}_q^T \mathbf{c}_q \boldsymbol{\Delta}_q} e^{-\frac{1}{2}\boldsymbol{\Delta}_p^T \mathbf{c}_p \boldsymbol{\Delta}_p}, \end{aligned} \tag{17}$$

with $\mathbf{\Delta}_q = \mathbf{q}_t' - \mathbf{q}_t$ and $\mathbf{\Delta}_p = \mathbf{p}_t' - \mathbf{p}_t$. The prefactor, D_t, is given by

$$\begin{aligned} D_t \; &= 2^{-\frac{N}{2}} \det(\gamma_0 \mathbf{G})^{\frac{1}{2}} \det \Big| \frac{1}{2}(\mathbf{M}^b_{pp} - i\gamma_0 \mathbf{M}^b_{qp})(\mathbf{G}^{-1} + \mathbb{I})(\mathbf{M}^f_{pp}\gamma_0 + i\mathbf{M}^f_{pq}) \\ &+ (\gamma_0 \mathbf{M}^b_{qq} + i\mathbf{M}^b_{pq})(\frac{1}{2}\gamma_t + \mathbf{c}_p)\mathbf{G}^{-1}(\mathbf{M}^b_{pp}\gamma_0 + i\mathbf{M}^f_{pq}) \\ &+ \frac{1}{2}(\mathbf{M}^b_{qq} + i\mathbf{M}^b_{pq})(\mathbf{G}^{-1} + \mathbb{I})(\mathbf{M}^f_{qq} - i\mathbf{M}^f_{qp}\gamma_0) \\ &+ (\mathbf{M}^b_{pp} - i\gamma_0 \mathbf{M}^b_{qp})(\frac{1}{2}\gamma_t + \mathbf{c}_q)\mathbf{G}^{-1}(\mathbf{M}^b_{qq} - i\mathbf{M}^f_{qp}\gamma_0) \Big|^{\frac{1}{2}}. \end{aligned} \tag{18}$$

Note that as $\mathbf{c}_p, \mathbf{c}_q \to 0$ we recover the original DHK-IVR, and as $\mathbf{c}_p, \mathbf{c}_q \to \infty$ we effectively perform a stationary phase approximation and obtain a result similar to the LSC-IVR involving Husimi distributions,

$$C_{AB}(t) \; = \; \frac{1}{(2\pi\hbar)^N} \int \mathrm{d}\mathbf{p}_0 \int \mathrm{d}\mathbf{q}_0 \, \langle \mathbf{p}_0\mathbf{q}_0|\hat{A}|\mathbf{p}_0\mathbf{q}_0\rangle \, \langle \mathbf{p}_t\mathbf{q}_t|\hat{B}|\mathbf{p}_t\mathbf{q}_t\rangle \,, \tag{19}$$

which we refer to as the Husimi-IVR. With intermediate values of $\mathbf{c}_p, \mathbf{c}_q$ one can select a set of tuning parameters that both reduces computational expense and recovers accurate quantum information. The following two subsections describe two implementations of the MQC-IVR.

3.2.1 Forward-Backward MQC-IVR

The first step in evaluating Eq. (17) is to sample the initial conditions of the forward trajectory $(\mathbf{p}_0, \mathbf{q}_0)$ as well as the phase space displacements at time t, $(\mathbf{\Delta}_p, \mathbf{\Delta}_q)$. For example, the models provided in this program define the initial state as a pure coherent state, $\hat{A} = |\mathbf{p}_i\mathbf{q}_i\rangle \langle \mathbf{p}_i\mathbf{q}_i|$, so the sampling distribution in this case looks like

$$\omega(\mathbf{p}_0, \mathbf{q}_0, \mathbf{\Delta}_p, \mathbf{\Delta}_q) \; = \; |\, \langle \mathbf{p}_0\mathbf{q}_0|\mathbf{p}_i\mathbf{q}_i\rangle \,|^2 e^{-\frac{1}{2}\mathbf{\Delta}_q^T \mathbf{c}_q \mathbf{\Delta}_q} e^{-\frac{1}{2}\mathbf{\Delta}_p^T \mathbf{c}_p \mathbf{\Delta}_p}. \tag{20}$$

The following diagram outlines how the program computes the dynamics of a single trajectory beginning at $(\mathbf{p}_0, \mathbf{q}_0)$. The initial point is propagated for a single time step Δt to point $(\mathbf{p}_t, \mathbf{q}_t)$, followed by an instantaneous jump in phase space to point $(\mathbf{p}_t', \mathbf{q}_t')$; this jump is due to the action of operator $\hat{B}$ on the system. Recall that, like the initial point, the jumps $(\mathbf{\Delta}_p, \mathbf{\Delta}_q)$ are sampled from Eq. (20). The new phase-space point $(\mathbf{p}_t', \mathbf{q}_t')$ is then propagated backward for time Δt (with a negative time step) to $(\mathbf{p}_0', \mathbf{q}_0')$.

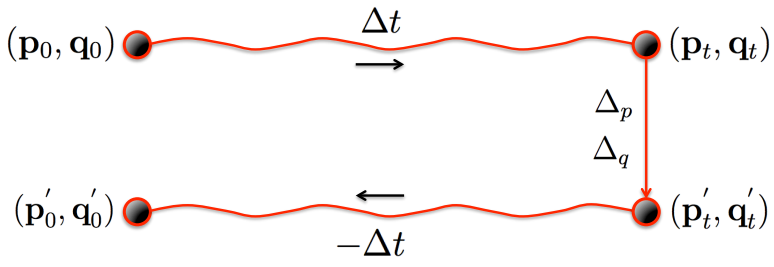

The phase space jumps and backward propagations to time $t = 0$ are subsequently repeated for each additional time step of the forward trajectory. The symplectic integrator (see below for details) is used to time evolve monodromy matrix elements and we evaluate the classical action along the classical trajectory pair. All of this dynamical information is then fed into subroutines that compute the phase,

prefactor, and matrix elements appearing in the integrand of the correlation function. The final result is then obtained by converging with respect to the number of sampled initial phase space points.

The dimensionality of the integral can be reduced if operator $\hat{B}$ is purely a function of the position or momentum operator. For example, when $\hat{B} = B(\hat{\mathbf{q}})$ we can collapse the coherent states at time t to position states by evaluating the following limit,

$$\lim_{\gamma_t \to \infty} \det(\gamma_t)^{\frac{1}{2}} \, \langle \mathbf{p}_t' \mathbf{q}_t' | B(\hat{\mathbf{q}}) | \mathbf{p}_t \mathbf{q}_t \rangle \;=\; (4\pi)^{\frac{N}{2}} \delta(\mathbf{\Delta}_q) B\left(\frac{\mathbf{q}_t' + \mathbf{q}_t}{2} \right). \tag{21}$$

After inserting (21) into (17) and evaluating the integral over $\mathbf{\Delta}_q$ we have

$$\begin{aligned} C_{AB}(t) \;&= 2^{-2N} \pi^{-\frac{3N}{2}} \int \mathrm{d}\mathbf{p}_0 \int \mathrm{d}\mathbf{q}_0 \int \mathrm{d}\mathbf{\Delta}_p \, e^{\frac{i}{\hbar}[S_t(\mathbf{p}_0,\mathbf{q}_0) + S_{-t}(\mathbf{p}_t,\mathbf{q}_t)]} \\ &\quad \times D_q(\mathbf{p}_0, \mathbf{q}_0, \mathbf{\Delta}_p; \mathbf{c}_p) \, \langle \mathbf{p}_0 \mathbf{q}_0 | \hat{A} | \mathbf{p}_0' \mathbf{q}_0' \rangle \, B(\mathbf{q}_t) e^{-\frac{1}{2} \mathbf{\Delta}_p^T \mathbf{c}_p \mathbf{\Delta}_p}, \end{aligned} \tag{22}$$

with the prefactor now given by

$$\begin{aligned} D_q(\mathbf{p}_0, \mathbf{q}_0, \mathbf{\Delta}_p; \mathbf{c}_p) \;=\; \det \Big| \gamma_0^{-1} \mathbf{c}_p \Big[&(\mathbf{M}_{pp}^b - i\gamma_0 \mathbf{M}_{qp}^b)(\mathbf{M}_{pp}^f \gamma_0 + i \mathbf{M}_{pq}^f) \\ &+ (\gamma_0 \mathbf{M}_{qq}^b + i \mathbf{M}_{pq}^b)(\mathbf{M}_{qq}^f - i \mathbf{M}_{qp}^f \gamma_0) \\ &+ (\mathbf{M}_{pp}^b - i\gamma_0 \mathbf{M}_{qp}^b) \mathbf{c}_p^{-1} (\mathbf{M}_{qq}^f - i \mathbf{M}_{qp}^f \gamma_0) \Big] \Big|^{\frac{1}{2}}. \end{aligned} \tag{23}$$

Only momentum jumps are imposed in this limit. Similarly, we can evaluate the limit that $\gamma_t \to 0$ to recover an expression when operator $\hat{B}$ is of the type $\hat{B} = B(\hat{\mathbf{p}})$,

$$\begin{aligned} C_{AB}(t) \;&= \frac{1}{(2\pi\hbar)^{2N}} \int \mathrm{d}\mathbf{p}_0 \int \mathrm{d}\mathbf{q}_0 \int \mathrm{d}\mathbf{\Delta}_q \, e^{\frac{i}{\hbar}[S_t(\mathbf{p}_0,\mathbf{q}_0) + S_{-t}(\mathbf{p}_t,\mathbf{q}_t)]} \\ &\quad \times D_p(\mathbf{p}_0, \mathbf{q}_0, \mathbf{\Delta}_q; \mathbf{c}_q) \, \langle \mathbf{p}_0 \mathbf{q}_0 | \hat{A} | \mathbf{p}_0' \mathbf{q}_0' \rangle \, B(\mathbf{p}_t) e^{-\frac{1}{2} \mathbf{\Delta}_q^T \mathbf{c}_p \mathbf{\Delta}_q}, \end{aligned} \tag{24}$$

with the prefactor

$$\begin{aligned} D_p(\mathbf{p}_0, \mathbf{q}_0, \mathbf{\Delta}_q; \mathbf{c}_q) \;=\; \det \Big| \gamma_0^{-1} \mathbf{c}_q \Big[&(\mathbf{M}_{pp}^b - i\gamma_0 \mathbf{M}_{qp}^b)(\mathbf{M}_{pp}^f \gamma_0 + i \mathbf{M}_{qp}^f) \\ &+ (\gamma_0 \mathbf{M}_{qq}^b + i \mathbf{M}_{pq}^b)(\mathbf{M}_{qq}^f - i \mathbf{M}_{qp}^f \gamma_0) \\ &+ (\gamma_0 \mathbf{M}_{qq}^b + i \mathbf{M}_{pq}^b) \mathbf{c}_q^{-1} (\mathbf{M}_{pp}^f \gamma_0 + i \mathbf{M}_{pq}^f) \Big] \Big|^{\frac{1}{2}}. \end{aligned} \tag{25}$$

When evaluating Eq. (22) the sampling distribution is the same as before, Eq. (20), but with $\mathbf{\Delta}_q \to 0$. Likewise when evaluating Eq. (24) use $\mathbf{\Delta}_p \to 0$.

3.2.2 Double-Forward MQC-IVR

It is far more efficient to propagate two independent trajectories forward in time than it is to apply the forward-backward method of the previous section. The MQC-IVR can be re-derived to exploit this efficiency. Begin by using Liouville's theorem, $\mathrm{d}\mathbf{p}_t' \mathrm{d}\mathbf{q}_t' = \mathrm{d}\mathbf{p}_0' \mathrm{d}\mathbf{q}_0'$, to rewrite the DHK-IVR,

$$\begin{aligned} C_{AB}(t) \;&= \frac{1}{(2\pi\hbar)^{2N}} \int \mathrm{d}\mathbf{p}_0 \int \mathrm{d}\mathbf{q}_0 \int \mathrm{d}\mathbf{p}_0' \int \mathrm{d}\mathbf{q}_0' \, e^{\frac{i}{\hbar}[S_t(\mathbf{p}_0,\mathbf{q}_0) - S_t(\mathbf{p}_0',\mathbf{q}_0')]} \\ &\quad \times C_t(\mathbf{p}_0, \mathbf{q}_0) \, C_t(\mathbf{p}_0', \mathbf{q}_0') \, \langle \mathbf{p}_0 \mathbf{q}_0 | \hat{A} | \mathbf{p}_0' \mathbf{q}_0' \rangle \, \langle \mathbf{p}_t' \mathbf{q}_t' | \hat{B} | \mathbf{p}_t \mathbf{q}_t \rangle \, . \end{aligned} \tag{26}$$

We now construct the Filinov damping factor to filter trajectory displacements at time zero rather than time t. The final result is given by

$$\begin{aligned} C_{AB}(t) \;=\; & \frac{1}{(2\pi\hbar)^{2N}} \int \mathrm{d}\mathbf{p}_0 \int \mathrm{d}\mathbf{q}_0 \int \mathrm{d}\mathbf{p}_0' \int \mathrm{d}\mathbf{q}_0'\, e^{\frac{i}{\hbar}[S_t(\mathbf{p}_0,\mathbf{q}_0)-S_t(\mathbf{p}_0',\mathbf{q}_0')]} \\ & \times D_t(\mathbf{p}_0,\mathbf{q}_0,\mathbf{p}_0',\mathbf{q}_0';\mathbf{c}_p,\mathbf{c}_q)\, \langle \mathbf{p}_0\mathbf{q}_0|\hat{A}|\mathbf{p}_0'\mathbf{q}_0'\rangle\, \langle \mathbf{p}_t'\mathbf{q}_t'|\hat{B}|\mathbf{p}_t\mathbf{q}_t\rangle \\ & \times e^{-\frac{1}{2}\boldsymbol{\Delta}_{q_0}^T \mathbf{c}_q \boldsymbol{\Delta}_{q_0}}\, e^{-\frac{1}{2}\boldsymbol{\Delta}_{p_0}^T \mathbf{c}_p \boldsymbol{\Delta}_{p_0}}. \end{aligned} \tag{27}$$

with $\boldsymbol{\Delta}_{p_0} = \mathbf{p}_0' - \mathbf{p}_0$ and $\boldsymbol{\Delta}_{q_0} = \mathbf{q}_0' - \mathbf{q}_0$, and the prefactor given by

$$\begin{aligned} D_t \;=\; & \det(\frac{1}{2}\gamma_t^{-1}\mathbf{G})^{\frac{1}{2}} \det\Big|\frac{1}{2}(\mathbf{M}_{pp}^f - i\gamma_t\mathbf{M}_{qp}^f)(\mathbf{G}^{-1}+\mathbb{I})(\mathbf{M}_{pp}^b\gamma_t + i\mathbf{M}_{pq}^b) \\ & +(\gamma_t\mathbf{M}_{qq}^f + i\mathbf{M}_{pq}^f)(\frac{1}{2}\gamma_0^{-1}+\mathbf{c}_p)\mathbf{G}^{-1}(\mathbf{M}_{pp}^b\gamma_t + i\mathbf{M}_{pq}^b) \\ & +\frac{1}{2}(\gamma_t\mathbf{M}_{qq}^f + i\mathbf{M}_{pq}^f)(\mathbf{G}^{-1}+\mathbb{I})(\mathbf{M}_{qq}^b - i\mathbf{M}_{qp}^b\gamma_t) \\ & +(\mathbf{M}_{pp}^f - i\gamma_t\mathbf{M}_{qp}^f)(\frac{1}{2}\gamma_0+\mathbf{c}_q)\mathbf{G}^{-1}(\mathbf{M}_{qq}^b - i\mathbf{M}_{qp}^b\gamma_t)\Big|^{\frac{1}{2}}. \end{aligned} \tag{28}$$

The limits of the tuning strength are identical to the forward-backward implementation, yielding Eq. (26) as $\mathbf{c}_p, \mathbf{c}_q \to 0$, and yielding the Husimi-IVR as $\mathbf{c}_p, \mathbf{c}_q \to \infty$. The following sampling distribution is used to generate mean ($\bar{x} = \frac{1}{2}(x_0' - x_0)$) and difference variables at time zero,

$$\omega(\mathbf{p}_0,\mathbf{q}_0,\mathbf{p}_0',\mathbf{q}_0') \;=\; |\,\langle \bar{\mathbf{p}}\,\bar{\mathbf{q}}|\mathbf{p}_i\mathbf{q}_i\rangle\,|^2 e^{-\frac{1}{2}\boldsymbol{\Delta}_{p_0}\mathbf{c}_p\boldsymbol{\Delta}_{p_0}}\, e^{-\frac{1}{2}\boldsymbol{\Delta}_{q_0}\mathbf{c}_q\boldsymbol{\Delta}_{q_0}}. \tag{29}$$

From these we can recover the initial points of a pair of trajectories, $(\mathbf{p}_0,\mathbf{q}_0)$ and $(\mathbf{p}_0',\mathbf{q}_0')$. Each of these points are then independently propagated forward in time and the time-dependent contributions to the semiclassical integrand evaluated along the classical trajectories as described for the Forward-Backward implementation.

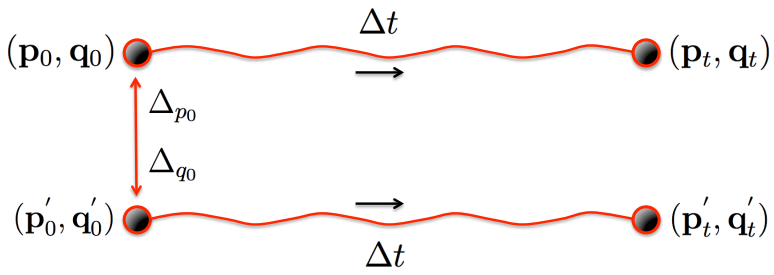

Under the previous forward-backward implementation, the total number of system moves (in positions and momenta) per trajectory pair goes as $\frac{1}{2}N(N_t^2+3N_t)$ for a system of N degrees of freedom and N_t time steps. With the Double-Forward implementation, however, the scaling goes as $2NN_t$: a significant improvement in computational expense.

4 Semiclassical Nonadiabatic Dynamics

One way of representing a discrete F-level system with continuous variables is with the Meyer-Miller-Stock-Thoss (MMST) Hamiltonian,

$$H = \frac{1}{2}\mathbf{P}^{\mathrm{T}}\mathbf{M}^{-1}\mathbf{P} + \frac{1}{2}\mathbf{p}^{\mathrm{T}}\mathbf{V}(\mathbf{R})\mathbf{p} + \frac{1}{2}\mathbf{x}^{\mathrm{T}}\mathbf{V}(\mathbf{R})\mathbf{x} - \frac{1}{2}\,\mathrm{Tr}\,[\mathbf{V}(\mathbf{R})]\,, \tag{30}$$

where $(\mathbf{P}, \mathbf{R})$ and $(\mathbf{x}, \mathbf{p})$ are nuclear and electronic phase space variables, respectively, $\mathbf{V}(\mathbf{R})$ is the $F \times F$ diabatic electronic potential energy matrix, $\mathbf{M}$ is a $G \times G$ diagonal matrix of nuclear masses, and G is the number of nuclear degrees of freedom. A consequence of representing electronic information with continuous variables in this way is that the continuous variables $(\mathbf{x}, \mathbf{p})$ are restricted to the singly-excited harmonic oscillator subspace. For example, the total wavefunction of a nuclear wavepacket, $|\phi\rangle$, occupying electronic state s in an F-level system is given by

$$|\Psi\rangle = |\phi\, 0_1 0_2 \ldots 1_s \ldots 0_F\rangle\,, \tag{31}$$

where the 0_λ or 1_λ is a zero or single harmonic excitation in oscillator λ, which represents electronic state λ.

The SC correlation functions outlined in the previous sections can easily be applied to systems evolved under the MMST Hamiltonian because each degree of freedom, both nuclear and electronic, is represented by a continuous phase space variable. The MInt algorithm for computing trajectories and the monodromy matrix with the MMST Hamiltonian is outlined in the following section.

4.1 The MInt Algorithm

It is known that when a Hamiltonian is decomposed to a sum of sub-Hamiltonians, a symmetric composition of exact evolutions under the sub-Hamiltonians results in approximate evolution under the total Hamiltonian that is exactly symplectic. By symplectic we mean that the following condition,

$$\mathbf{M}^{\mathrm{T}}\mathbf{J}^{-\mathbf{1}}\mathbf{M} = \mathbf{J}^{-\mathbf{1}}, \tag{32}$$

where $\mathbf{M}$ is the monodromy matrix and $\mathbf{J}$ is the structure matrix,

$$\mathbf{J} = \begin{pmatrix} \mathbb{O} & \mathbb{I} \\ -\mathbb{I} & \mathbb{O} \end{pmatrix}, \tag{33}$$

is conserved exactly. We therefore split Eq. (30) into two parts,

$$H = H_1 + H_2 \tag{34}$$

$$H_1 = \frac{1}{2}\mathbf{P}^{\mathrm{T}}\mathbf{M}^{-\mathbf{1}}\mathbf{P} \tag{35}$$

$$H_2 = \frac{1}{2}\mathbf{p}^{\mathrm{T}}\mathbf{V}(\mathbf{R})\mathbf{p} + \frac{\mathbf{1}}{\mathbf{2}}\mathbf{x}^{\mathrm{T}}\mathbf{V}(\mathbf{R})\mathbf{x} - \frac{\mathbf{1}}{\mathbf{2}}\,\mathrm{Tr}\left[\mathbf{V}(\mathbf{R})\right], \tag{36}$$

and define the following flow map,

$$\Psi_{H,\Delta t} = \Phi_{H_1,\Delta t/2} \circ \Phi_{H_2,\Delta t} \circ \Phi_{H_1,\Delta t/2}, \tag{37}$$

which defines the propagation scheme. The notation uses $\Phi_{H_i,t}$ to represent exact evolution under Hamiltonian H_i for time t, $\Phi_{H_i,t}(\mathbf{z_0}) = \mathbf{z_t}$, and the circles represent the composition operation: $f \circ g(z) = f(g(z))$. In words, Eq. (37) says we propagate the system under H_1 for half a timestep, followed by evolution under H_2 for a full timestep, and under H_1 again for another half timestep. So long as the sub-evolutions are exact the total evolution, $\Psi_{H,\Delta t}$, will be exactly symplectic. Hamilton's equations are therefore solved according to the scheme in Eq. (37). See reference 8 of Section 1.1 for a complete derivation of the equations of motion for the phase space variables and monodromy matrix.

5 SC-IVR Code Package

5.1 Program Overview

The package contains a collection of FORTRAN programs that compute the SC-IVR correlation functions of Eqs. (13), (14), (17), (19), (22), (24) and (27) for 1D, multidimensional, and nonadiabatic systems. The input file `theory.in` allows you to choose which SC-IVR to use, and defines all simulation parameters one would need. We provide three adiabatic model systems that may serve as a template for other systems of your choosing; the harmonic oscillator,

$$V(x) \;=\; \frac{1}{2}m\omega^2 x^2, \tag{38}$$

an anharmonic oscillator

$$V(x) \;=\; \frac{1}{2}m\omega^2 x^2 - 0.1x^3 + 0.1x^4, \tag{39}$$

and a 2D system-bath model where Eq. (39) is coupled to a harmonic mode

$$V(x,y) \;=\; \frac{1}{2}m_x\omega_x^2 x^2 - 0.1x^3 + 0.1x^4 + \frac{1}{2}m_y\omega_y^2 y^2 + kxy. \tag{40}$$

Also included is a nonadiabatic model system with two electronic states and one nuclear degree of freedom. Elements of the diabatic electronic potential energy matrix for this system are given by

$$\mathbf{V}_{11}(R) = V_0\left[1 + \tanh\left(\alpha R\right)\right] \tag{41}$$

$$\mathbf{V}_{22}(R) = V_0\left[1 - \tanh\left(\alpha R\right)\right] \tag{42}$$

$$\mathbf{V}_{12}(R) = ae^{-bR^2}, \tag{43}$$

with parameters specified in the program.

For the adiabatic model systems, the program computes a quantity of the form

$$\langle B\rangle_t \;=\; \langle \mathbf{p}_i\mathbf{q}_i|e^{\frac{i}{\hbar}\hat{H}t}\hat{B}e^{-\frac{i}{\hbar}\hat{H}t}|\mathbf{p}_i\mathbf{q}_i\rangle\,, \tag{44}$$

which is Eq. (10) with an initial coherent state projection for operator $\hat{A} = |\mathbf{p}_i\mathbf{q}_i\rangle\langle\mathbf{p}_i\mathbf{q}_i|$. With the provided models, you have the choice of taking $\hat{B} = \hat{\mathbf{q}}$ or $\hat{B} = \hat{\mathbf{p}}$. In the nonadiabatic model system, the program computes the particle's momentum distribution after it traverses the crossing region,

$$C(P_f) = \lim_{t\to\infty}\langle P_{Ri}R_i1_10_2|\delta(P_f - \hat{P})|P_{Ri}R_i1_10_2\rangle\,, \tag{45}$$

given that the initial state of the system is a nuclear coherent state occupying electronic state 1.

5.2 Running the Program

Here, we assume a UNIX or Windows-X or MAC-OSX terminal environment. In the parent directory, specify the SC-IVR of your choice as well as your input parameters in the file `theory.in`, and then execute the bash script `execute.sh`. This will generate a directory called `EXPERIMENT` which contains the program you specified. Typing `make` while in the `EXPERIMENT` directory will compile the program and generate an executable file `dyn.x`. To run the program, type `./dyn.x` to start the simulation. All system parameters in the `input_1D` (`input_mD`) file can be edited without having to recompile the program, but changing the first five system options will do nothing while you are in the `EXPERIMENT` directory; these can only be specified in the parent directory.

If you intend to parallelize the calculation with MPI, then use `jobrun.sh` to submit the script (see below, this script will need to be edited according to your computational resources). Note that executing the bash script again will overwrite the existing `EXPERIMENT` directory, so it should be renamed to be safe. When the simulation is complete, a file named `TCF.out` will contain the real and imaginary parts of the correlation function as a function of time, and a file named `MC.configs` contains the initial phase space configurations of the classical trajectories.

5.3 The Makefile, External Libraries, and the MPI Submission Script

In the directory `makefiles` is a universal makefile. When the script `execute.sh` is run, the makefile is copied into the `EXPERIMENT` directory, and a simple search-and-replace routine tailors the makefile to your specifications. Depending on your operating system, the makefile may need to be edited. Note that we specify paths to the LAPACK and BLAS libraries, and mpif90 is used as well. Also note that we do NOT encourage you to edit the names of any FORTRAN files, modules or scripts that do not sit in the `EXPERIMENT` directory, as this may prevent the program from assembling the `EXPERIMENT` directory appropriately.

In the directory `Scripts` there is a submission script called `jobrun.sh`. This uses the Portable Batch System (PBS) scheduler, and will need to be edited if another scheduler is used.

5.4 Tutorial 1: 1D Anharmonic Oscillator

In the parent directory, set up the input file `theory.in` to compute the average position of the anharmonic oscillator with the Husimi-IVR.

```
Degrees of freedom
1
Level of theory ( ...
2
Implementation ( ...
1
Type of observable ( ...
1
Model Potentials ( ...
2
List the diagonal ...
1.0
List the coherent state and ...
1.0     0.0     1.414     1.414     10.0     10.0
Timestep, number of timesteps, ...
0.05     1400     1e-5
Number of trajectories
120000
```

Leave an arbitrary number for the tuning parameters when the MQC-IVR is not being used, in this case we use 10.0. Also, even though the `Implementation` line is irrelevant in this case, leave it as 1 for the Husimi and LSC-IVRs. Execute the bash script with `sh execute.sh`. This generates a directory called `EXPERIMENT` which contains the program specified by the input file. Rename the `EXPERIMENT` directory and `cd` into it. There are several FORTRAN files in the experiment directory. The input file in this directory is called `input_1D`: a copy of the `theory.in` file from the parent directory. The file `MonteCarlo_1D.f90` contains subroutines that generate initial configurations for each of the 1D implementations, `params_1D.f90` contains the global parameters and a subroutine that reads the input file, `traj_1D.f90` contains subroutines that propagate the classical trajectories (depending upon the

type of SC-IVR), `potential_1D.f90` contains the model potentials, `jobrun.sh` is a submission script for jobs using MPI, and `supply_1D.f90` contains a symplectic integrator and various subroutines that compute matrix elements and prefactors. The file `HUS_timecorr_1D.f90` contains the program which computes the correlation function, drawing upon the subroutines that you originally specified in `theory.in`. Note that the default potential parameters (in this case the frequency ω) are hard-coded in the potential subroutine of the file `potential_1D.f90`. Start the simulation with `./dyn.x` ($\sim$ 20sec) and plot the real part of the result contained in the file `TCF.out`. This should resemble the following figure.

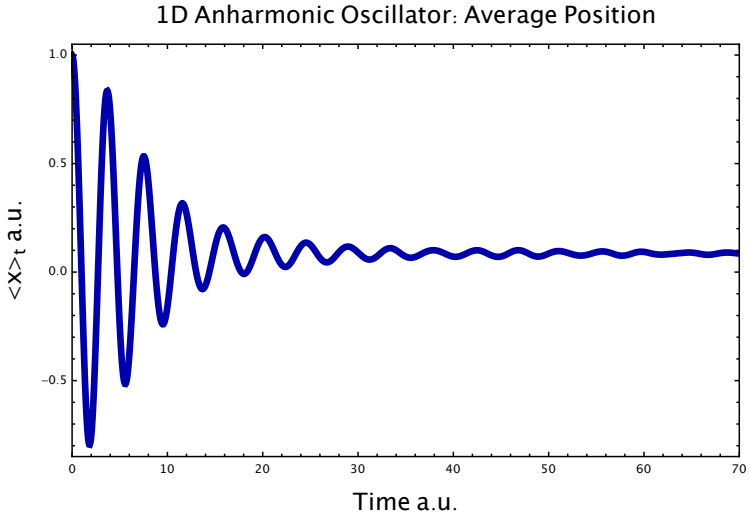

Now go back to the parent directory and start a new experiment, identical to the previous one but with the Double-Forward MQC-IVR and $c_p = c_q = 10$. The input file `theory.in` should read

```
Degrees of freedom
1
Level of theory ( ...
3
Implementation ( ...
1
Type of observable ( ...
1
Model Potentials ( ...
2
List the diagonal ...
1.0
List the coherent state and ...
1.0     0.0     1.414     1.414      10.0     10.0
Timestep, number of timesteps, ...
0.05    1400     1e-5
Number of trajectories
120000
```

Compile and run the program as before ($\sim$ 1min) and compare the two results. The large amplitudes at later times should be apparent in the MQC-IVR result, as shown in the figure below. This is characteristic of the exact quantum result, which the MQC-IVR approaches as the $\mathbf{c}_p, \mathbf{c}_q \to 0$. This limit however requires

more trajectories.

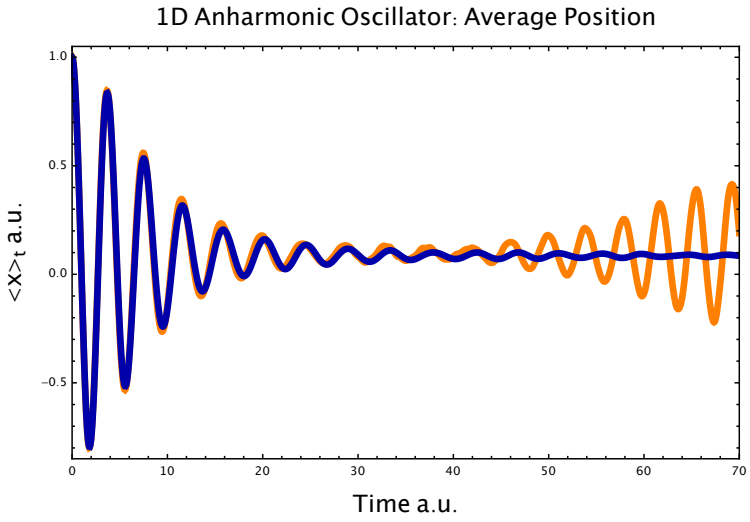

5.5 Tutorial 2: 2D Anharmonic Oscillator

Now we will compute the average momentum of an anharmonic oscillator that is coupled to a heavy harmonic mode with the Husimi-IVR. Recall that the potential energy parameters (in this case the two frequencies and coupling constant) are hard-coded into the potential energy subroutine. The `theory.in` file should read

```
Degrees of freedom
2
Level of theory ( ...
2
Implementation ( ...
1
Type of observable ( ...
2
Model Potentials ( ...
2
List the diagonal ...
1.0     25.0
List the coherent state and ...
1.0     0.0     1.414     1.414      10.0     10.0
1.0     0.0     8.333     8.333      10.0   10.0
Timestep, number of timesteps, ...
0.05    1400     1e-5
Number of trajectories
36000
```

With this input file, generate an `EXPERIMENT` directory, compile, run the simulation ($\sim$ 1min), and plot the result in `TCF.out`. The real part is plotted in the following figure.

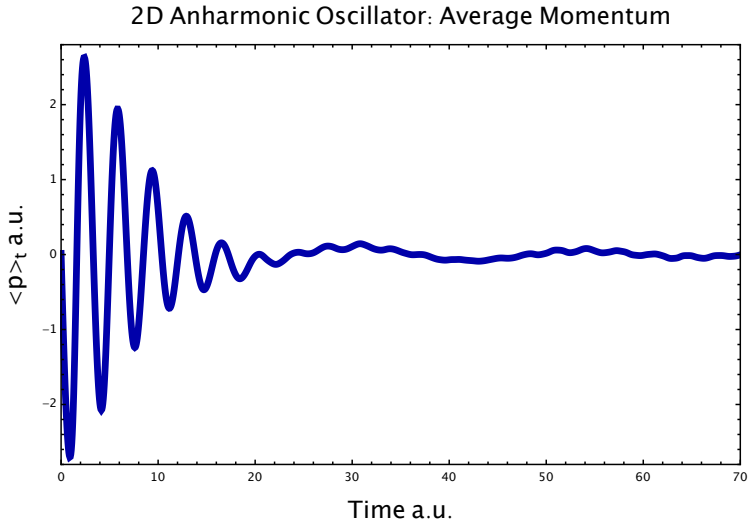

In order to observe the average momentum of the harmonic mode of this system rather than the anharmonic mode, `vi` into the file `HUS_timecorr_mD.f90` and change the `doflabel` in line 37 from 1 to 2. Re-compile with `make` and then run the simulation. The real part of the output is shown in the following figure.

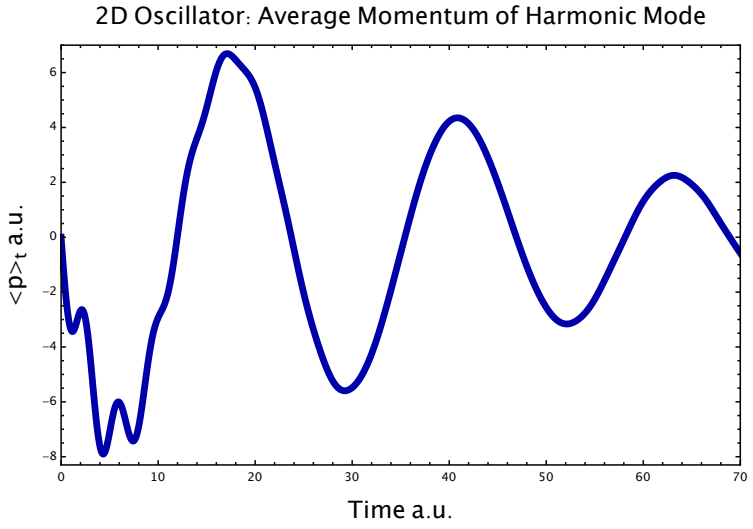

5.6 Altering the Code

We do not advise that you alter any files, directories, or scripts unless they created in an `EXPERIMENT` directory. In order to design your own experiment, it is suggested that you use `theory.in` to generate an `EXPERIMENT` directory with the SC-IVR of your choosing with an arbitrary model potential. Then while working in the `EXPERIMENT` directory you have the freedom to alter the potential and any subroutine you may wish to edit. The next two tutorials suggest how an original experiment can be created.

5.6.1 Tutorial 3: Other Potentials

We wish to calculate the average position of the anharmonic oscillator which is now coupled to two identical harmonic bath modes. We'll use the Double-Forward MQC-IVR and a large tuning parameter to set up `theory.in` as follows.

```
Degrees of freedom
3
Level of theory ( ...
3
Implementation ( ...
1
Type of observable ( ...
1
Model Potentials ( ...
2
List the diagonal ...
1.0     25.0     25.0
List the coherent state and ...
1.0     0.0     1.414     1.414      1000      1000
1.0     0.0     8.333     8.333      1000      1000
1.0     0.0     8.333     8.333      1000      1000
Timestep, number of timesteps, ...
0.05    1400     1e-5
Number of trajectories
36000
```

Generate an `EXPERIMENT` directory with this input file and `cd` into it. The program will compile but the potential energy subroutine needs to account for the third body. This is found in `potential_mD.f90`; `vi` into this file and edit the potential to include the second harmonic mode. Use the same potential parameters as the other bath mode. The subroutine should now read

```
v = x(1)**2 - 0.1d0*x(1)**3 + 0.1d0*x(1)**4   &
     + 0.5d0*ky*x(2)**2 + coupling*x(1)*x(2)  &
     + 0.5d0*ky*x(3)**2 + coupling*x(1)*x(3)

dv(1) = 2.d0*x(1) - 0.3d0*x(1)**2 + 0.4d0*x(1)**3 &
          + coupling*x(2) + coupling*x(3)
dv(2) = ky*x(2) + coupling*x(1)
dv(3) = ky*x(3) + coupling*x(1)

d2v(1,1) = 2.d0 - 0.6d0*x(1) + 1.2d0*x(1)**2
d2v(1,2) = coupling
d2v(1,3) = coupling
d2v(2,1) = coupling
d2v(2,2) = ky
d2v(2,3) = 0.d0
d2v(3,1) = coupling
d2v(3,2) = 0.d0
d2v(3,3) = ky
```

Compile and run the program ($\sim$ 4min). The real part of the output should look as follows.

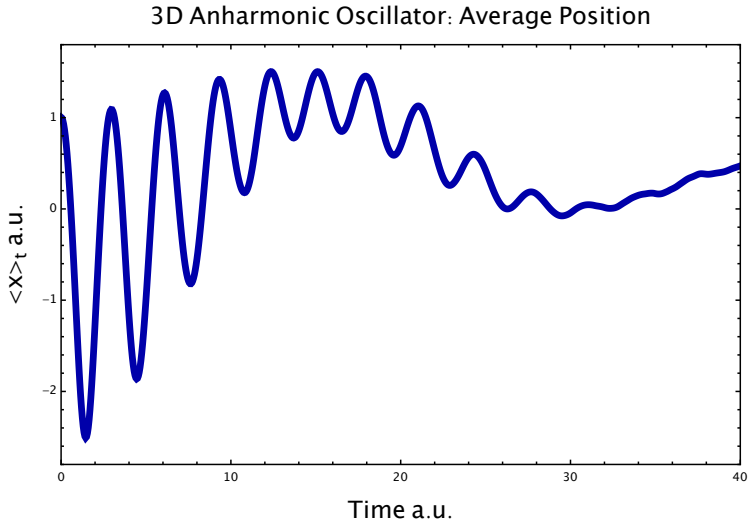

5.6.2 Tutorial 4: Other Observables

If the observable you wish to use is not one of the two provided ($\hat{\mathbf{p}}$ or $\hat{\mathbf{q}}$), then expressions for the following must be derived and coded into the program.

$\langle \mathbf{p}_t' \mathbf{q}_t' \vert \hat{B} \vert \mathbf{p}_t \mathbf{q}_t \rangle$	(FF-MQC-IVR, DHK-IVR)
$\langle \mathbf{p}_t \mathbf{q}_t \vert \hat{B} \vert \mathbf{p}_t \mathbf{q}_t \rangle$	(HUSIMI-IVR)
$B_w(\mathbf{p}_t, \mathbf{q}_t)$	(LSC-IVR)
$B(\mathbf{p}_t, \mathbf{q}_t)$	(FB-MQC-IVR)

The subroutines in the `supply_*.f90` files can be edited for this purpose if you don't wish to write your own. For example, repeat the calculation from the previous tutorial but use $\hat{B} = \hat{x}^2$ rather than $\hat{x}$. To evaluate the matrix element, insert a complete set of position states and evaluate the integral analytically,

$$\begin{aligned}
\langle \mathbf{p}_t' \mathbf{q}_t' \vert \hat{x}^2 \vert \mathbf{p}_t \mathbf{q}_t \rangle &= \int \mathrm{d}\mathbf{x} \, \langle \mathbf{p}_t' \mathbf{q}_t' \vert \hat{x}^2 \vert \mathbf{x} \rangle \, \langle \mathbf{x} \vert \mathbf{p_t} \mathbf{q_t} \rangle \\
&= \langle p_{zt}^{'} z_t^{'} \vert p_{zt} z_t \rangle \, \langle p_{yt}^{'} y_t^{'} \vert p_{yt} y_t \rangle \int \mathrm{d}x \; x^2 \, \langle p_{xt}^{'} x_t^{'} \vert x \rangle \, \langle x \vert p_{zt} z_t \rangle \\
&= \frac{1}{4} \left(\frac{2}{\gamma_x} - \frac{1}{\gamma_x^2} \left(p_{tx}^{'} - p_{tx} + i(q_{tx} + q_{tx}^{'}) \gamma_x \right)^2 \right) \langle \mathbf{p}_t' \mathbf{q}_t' \vert \mathbf{p}_t \mathbf{q}_t \rangle \, ,
\end{aligned}$$

where we have used both Eq. (7) and Eq. (9). The code near line 132 of `supply_mD.f90` should now be edited to look something like the following.

```
Bq = 0.25d0*(2.d0/WidthT(1,1)-(pp(1)-p(1)+Iu*(q(1)+qp(1))&
     *WidthT(1,1))**2/WidthT(1,1)**2)&
     *dexp(-0.25d0*dot_product(q-qp,q1)-0.25d0*dot_product(p-pp,p1))&
     *cdexp(-0.5d0*Iu*dot_product(p+pp,q-qp))
```

Compile and run the program, the output is plotted in the following figure.

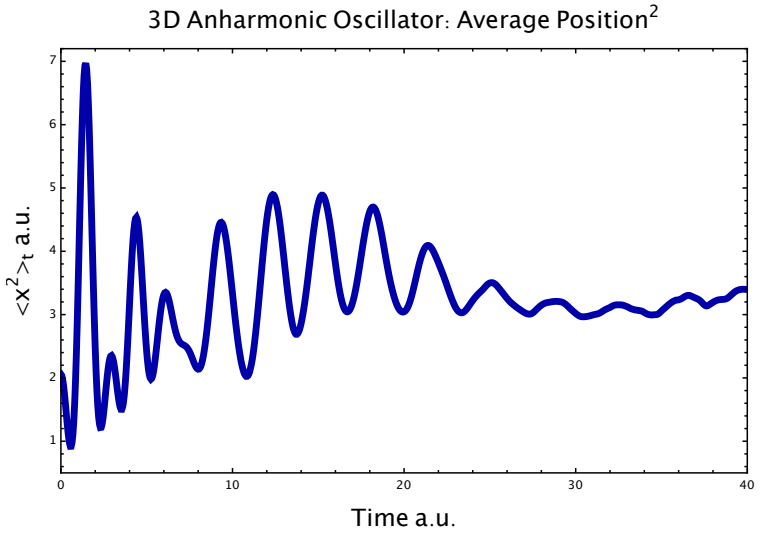

5.7 Tutorial 5: Nonadiabatic Dynamics with MQC-IVR

An `EXPERIMENT` directory containing the model nonadiabatic system and the double-forward MQC-IVR implementation can be created simply by entering `-1` under `Degrees of freedom` in the `theory.in` file.

```
Degrees of freedom
-1
```

Running the script `execute.sh` will then generate the `EXPERIMENT` directory containing the appropriate program. Note that it is typical of a semiclassical calculation of nonadiabatic systems to require a large number of trajectories to converge. So a quantum-limit calculation with MQC-IVR will require parallelization. See reference 8 of section 1.1 for convergence requirements.

5.8 The `MonteCarlo` files

In each of the `MonteCarlo` subroutines we use a Gaussian random number generator to produce initial configurations. The function `gauss` takes in the standard deviation σ of the sampling distribution and outputs a phase-space point. For example, the following sampling distribution is used with the 1D Husimi-IVR,

$$\omega(p_0, q_0) \;=\; \frac{1}{2\pi} e^{-\frac{\gamma_0}{2}(q_0 - q_i)^2} e^{-\frac{1}{2\gamma_0}(p_0 - p_i)^2}. \tag{46}$$

So the use of

```
gauss(1/dsqrt(Width0)) + qIn
```

and

```
gauss(dsqrt(Width0)) + pIn
```

generates the sampled points q_0 and p_0, respectively, from Eq. (46). Note that the normalization constant is either hard-coded into the `timecorr` files, or absent all together if it cancels with constants that appear in the correlation function. In the present case of the 1D Husimi-IVR it is absent altogether.

5.9 The `supply` files

The `supply` files contain formulas for the coherent state overlap Eq. (9), the matrix elements of the default observables, all SC-IVR prefactors, a fourth-order symplectic integrator, and an MPI initialization subroutine.

5.10 The `traj` files

The `traj` files contain three subroutines that take in an initial phase space point and output arrays containing trajectories, classical action, and monodromy matrix elements at each time step. Most of the provided SC-IVR methods use the subroutine `PropagateFwd_FF` to accomplish this, the otherwo are specifically used for the FB-MQC-IVR. Each of the three subroutines are configured to signal a flag when energy conservation or symplecticity breaks to within a small tolerance that is specified in the input file (default 10^{-5}). A flagged trajectory is halted and removed from the statistics.

5.11 Other comments

When running `execute.sh`, certain combinations of system options in `theory.in` will signal a flag. For example, a momentum-space LSC-IVR is not configured yet, so the script will notify you that this is not an option. Other than that example, all flags are due to minor subtleties, and will suggest to you how to proceed.

6 Acknowledgements

We acknowledge Dr. Sergey Antipov for providing version 1 of the MQC-IVR code, Srinath Ranya for comprehensive testing of the current implementation, and Dr. Timothy J. H. Hele for provided version 1 of the MInt algorithm code. We further acknowledge ARO (Grant No. W911NFD-13-1-0102) for funding.